Transforming Growth Factor–β Regulates Mammary Carcinoma Cell Survival and Interaction with the Adjacent Microenvironment

Brian Bierie,[1] Daniel G. Stover,[2] Ty W. Abel,[3] Anna Chytil,[1,4] Agnieszka E. Gorska,[1,4] Mary Aakre,[1,4] Elizabeth Forrester,[1] Li Yang,[1] Kay-Uwe Wagner,[5] and Harold L. Moses[1,2,4]

Departments of [1]Cancer Biology, [2]Medicine, and [3]Pathology and [4]Vanderbilt-Ingram Cancer Center, Vanderbilt University, Nashville, Tennessee and [5]Eppley Institute for Research in Cancer and Allied Diseases, University of Nebraska Medical Center, Omaha, Nebraska

Abstract

Transforming growth factor (TGF)–β signaling has been associated with early tumor suppression and late tumor progression; however, many of the mechanisms that mediate these processes are not known. Using Cre/LoxP technology, with the *whey acidic protein* promoter driving transgenic expression of Cre recombinase (WAP-Cre), we have now ablated the type II TGF-β receptor (TβRII) expression specifically within mouse mammary alveolar progenitors. Transgenic expression of the polyoma virus middle T antigen, under control of the mouse mammary tumor virus enhancer/promoter, was used to produce mammary tumors in the absence or presence of Cre ($T\beta RII^{(fl/fl);PY}$ and $T\beta RII^{(fl/fl);PY;WC}$, respectively). The loss of TGF-β signaling significantly decreased tumor latency and increased the rate of pulmonary metastasis. The loss of TGF-β signaling was significantly correlated with increased tumor size and enhanced carcinoma cell survival. In addition, we observed significant differences in stromal fibrovascular abundance and composition accompanied by increased recruitment of $F4/80^+$ cell populations in $T\beta RII^{(fl/fl);PY;WC}$ mice when compared with $T\beta RII^{(fl/fl);PY}$ controls. The recruitment of $F4/80^+$ cells correlated with increased expression of known inflammatory genes including *Cxcl1, Cxcl5*, and *Ptgs2* (cyclooxygenase-2). Notably, we also identified an enriched $K5^+$ $dNp63^+$ cell population in primary $T\beta RII^{(fl/fl);PY;WC}$ tumors and corresponding pulmonary metastases, suggesting that loss of TGF-β signaling in this subset of carcinoma cells can contribute to metastasis. Together, our current results indicate that loss of TGF-β signaling in mammary alveolar progenitors may affect tumor initiation, progression, and metastasis through regulation of both intrinsic cell signaling and adjacent stromal-epithelial interactions *in vivo*. [Cancer Res 2008;68(6):1809–19]

Introduction

The transforming growth factor β (TGF-β) ligands TGF-β1, TGF-β2, and TGF-β3 are potent regulators of cell behavior, and their activity can significantly regulate processes involved in tumor initiation, progression, and metastasis (1–4). TGF-β signaling pathways are altered in a large number of human cancers including those in the breast (5). Currently, a diverse repertoire of tumor cell–autonomous and tumor cell–independent mechanisms for the regulation of carcinoma initiation and progression by TGF-β *in vitro* and *in vivo* have been described (4, 6). TGF-β in normal epithelium is known to induce arrest of the cell cycle in G_1, and it has been suggested that this cytostatic mechanism is important for the suppression of tumor initiation and early tumor progression (7). In later stages of tumor progression, TGF-β signaling in the tumor microenvironment is thought to enhance tumor progression (1, 4). TGF-β stimulation in some normal and carcinoma-associated epithelial cell populations is known to induce an epithelial-to-mesenchymal transition that, in the context of a tumor microenvironment, may enhance carcinoma cell migration and invasion to promote metastasis (1, 4). Together, these observations suggest that TGF-β functions as a tumor suppressor or tumor promoter depending on the context of stimulation. However, many of the early studies were not able to control for local and systemic influences of exogenous TGF-β expression in the mammary tumor microenvironment.

TGF-β signaling has an effect on many cell types within the tumor microenvironment, and it is clear that some of the regulation occurs through direct control of tumor cells *in vivo*. Attenuation of TGF-β signaling in the mammary epithelium has been shown to result in lobular alveolar hyperplasia and decreased tumor latency in the presence of oncogenic stimuli (8, 9). Attenuation of TGF-β signaling in mammary carcinoma cells also resulted in decreased pulmonary metastasis whereas activation of the pathway specifically within mammary carcinoma cells increased metastasis (10, 11). The results obtained using transgenic dominant negative type II TGF-β receptor attenuation of TGF-β signaling suggested that a significant carcinoma cell–autonomous role for TGF-β signaling in breast cancer was the cytostatic suppression of early tumor progression and later promotion of tumor progression through enhanced carcinoma cell invasion and metastasis (12, 13). This dogmatic view of TGF-β signaling was subsequently modified when type II TGF-β receptor (TβRII) expression was completely ablated in mice. It was shown that attenuation of TGF-β signaling produced results that were different from those obtained with the complete tissue specific ablation of TβRII expression *in vivo* (14). Importantly, when TβRII was completely ablated in the mouse mammary tumor virus (MMTV)-PyVmT mouse model, there was a decrease in tumor latency with a dramatic increase in lung metastases (14).

However, off-target effects of TβRII deletion using the MMTV-Cre transgene included a wasting syndrome and spontaneous morbidity due to currently unknown systemic influences of TGF-β signaling (14). Therefore, a more specific approach was necessary to accurately determine the effect and mechanisms for enhanced tumor growth and metastasis when carcinoma cell TGF-β signaling responses were lost *in vivo*. To address this issue, we have implemented a strategy to specifically target the MMTV-PyVmT

Note: Supplementary data for this article are available at Cancer Research Online (http://cancerres.aacrjournals.org/).

Requests for reprints: Harold L. Moses, Department of Cancer Biology, Vanderbilt University, 698 Preston Research Building, 2220 Pierce Avenue, Nashville, TN 37232-6838. Phone: 615-936-1782; Fax: 615-936-1790; E-mail: hal.moses@vanderbilt.edu.

doi:10.1158/0008-5472.CAN-07-5597

mammary tumor progenitor cells using WAP-Cre–mediated deletion of TβRII *in vivo*. Using this strategy, we have been able to show that TGF-β signaling regulates tumor cell survival, composition of the adjacent fibrovascular stroma, recruitment of F4/80$^+$ bone marrow–derived cells, and inflammatory gene expression within the MMTV-PyVmT mammary tumor microenvironment.

Materials and Methods

Mouse models. TβRII$^{(fl/fl)}$ mice were crossed with MMTV-PyVmT, WAP-Cre, MMTV-Cre, and Rosa26R$^{(fl/fl)}$ transgenic mice to produce the TβRII$^{(fl/fl);PY}$, TβRII$^{(fl/fl);PY;WC}$, TβRII$^{(fl/fl);PY;WC}$Rosa26$^{(fl/fl)}$, and TβRII$^{(fl/fl);PY;MC}$ lines used for analysis (15–19). Mice were housed and handled according to approved Institutional Animal Care and Use Committee protocols. 5-Bromo-4-chloro-3-indolyl-β-D-galactopyranoside (X-Gal) staining was done using standard protocols.

Preparation of lung whole mounts. Lungs were removed and fixed in 10% NBF overnight at 4°C. The next day, lungs were dehydrated, placed in xylene for 1 h, and then changed to fresh xylene overnight. Lungs were rehydrated and then placed under running tap water for 30 min. The tissues were dipped in Mayer's hematoxylin for 2 min and then washed in running tap water for 5 min. Tissues were destained in HCl (fresh 1% v/v from a 12 N solution) for 20 min, rinsed in running tap water overnight, dehydrated, and placed in xylene overnight.

Immunohistochemistry and immunofluorescence. Immunohistochemistry and immunofluorescence were conducted using standard protocols (available on request). All immunohistochemistry and immunofluorescence protocols were blocked and incubated in the presence of normal horse serum (Vector Laboratories). Briefly, smooth muscle actin (SMA; DAKO), vimentin (DAKO), and p63 (Lab Vision; 1:200) immunohistochemistry was conducted as described in the manufacturer's protocol. Immunohistochemistry for von Willebrand factor (vWF) was done with a standard pH 8 EDTA epitope retrieval buffer. Immunohistochemistry and immunofluorescence for phospho-histone 3 (UBI; 1:1,000), cytokeratin 5 (K5; Covance; 1:5,000 immunohistochemistry, 1:1,000 immunofluorescence), dNp63 (Santa-Cruz; 1:200), cytokeratin 8 (K8; Developmental Studies Hybridoma Bank at the University of Iowa TROMA-1; 1:1,000), and SMA (immunofluorescence; Calbiochem, mAb 1 *A*4; 1:1,000) was done using a standard pH 6 sodium citrate buffer. Immunohistochemistry for CD31 (optimum cutting temperature compound frozen sections) and F4/80 (paraffin embedded) was done by the Vanderbilt Immunohistochemistry Core Facility. (Note: Due to the low abundance of dNp63, it was essential to use the blue or red wavelength for immunofluorescence detection to eliminate background autofluorescence.) Quantitation of relative pixel density for immunohistochemistry was done using the histogram function in Adobe Photoshop CS3 after thresholding and inversion of the black and white images obtained from individual RGB channels. Specifically, the blue channel was used for quantitation of positive immunohistochemistry signals to more accurately localize the brown stain before thresholding (the blue channel was used to produce grayscale images while eliminating a majority of signal from the blue hematoxylin counterstain before thresholding). Values obtained were normalized to total tumor tissue present in each image (histogram values for inverted threshold images obtained from the red channel) and reported as a ratio of the value for specific immunohistochemistry divided by total tissue present in each image (relative pixel density).

ApopTag analysis. Rehydrated paraffin-embedded tissue sections were washed thrice for 5 min in PBS, incubated for 20 min with 0.3% H_2O_2, washed thrice for 5 min in PBS, and then subjected to the rest of the ApopTag Peroxidase In Situ Apoptosis Detection Kit (Chemicon) protocol starting with incubation in TdT buffer as described by the manufacturer. Quantitation was done as described for immunohistochemistry.

Protein preparation and blotting. Protein collection and blotting techniques have previously been described (14); however, the following buffer was used for lysis: 50 mmol/L Tris (pH 7.5), 150 mmol/L NaCl, 10 mmol/L EDTA (pH 8.0), 0.2% sodium azide, 50 mmol/L NaF, and 0.5% NP40; Sigma inhibitor cocktails (P2850, P5726, and P8340) were added at 1:100 fresh. Proteins were prepared for loading by mixing 40 μg of protein with Laemmli sample buffer (Bio-Rad) and BME (5% final concentration). Primary antibodies TβRII (Santa Cruz L-21; 1:1,000), p-Smad3 (kind gift from Dr. Ed Leof, Department of Biochemistry and Molecular Biology, Mayo Clinic College of Medicine, Rochester, MN; 1:8,000), β-actin (Sigma; 1:4,000); cyclin D1 (Santa Cruz; 1:1,000), cyclin D2 (Santa Cruz; 1:1,000), and cleaved poly(ADP-ribose) polymerase 1 (PARP-1; Cell Signaling; 1:1,000) were incubated on the membranes for 2 h room temperature. The Smad3 antibody (Zymed; 1:500) was incubated on the membranes overnight at 4°C.

Cytokine antibody array. Cells were isolated as previously described (14) and cultured in complete medium (5% ABS). Sample collection, incubation, and detection were done as outlined in the manufacturer's protocol (Raybiotech, Inc.).

RNA preparation and real-time PCR. RNA was collected using Trizol reagent and then Dnase treated following the manufacturer's protocols (Invitrogen and Promega, respectively). RNA samples were further purified using the RNeasy Mini Kit (Qiagen). cDNA was prepared using Superscript II reverse transcriptase as described by the manufacturer (Invitrogen). Primers used for SYBR green (Bio-Rad) based real-time PCR analyses were Cxcl1 (20), Cxcl5 (20), Cxcl16 (20), Ccl5 (21), Ccl9 (21), Ccl20 (21), Ptgs2 (22), and 18S (F, 5′-CAAGAACGAAAGTCGGAGGTTC-3′; R, 5′-GGACATC-TAAGGGCATCACAG-3′). Samples were run on a Bio-Rad iCyclerIQ and the C_t values were subjected to statistical analyses after normalization to 18S and transformation to the median.

Results

Loss of TβRII in mammary tumor progenitor cells significantly decreased tumor latency while increasing tumor burden and pulmonary metastases. To mediate recombination in the mammary gland, we used the WAP gene promoter to drive expression of Cre recombinase *in vivo* (17). In contrast to the MMTV-Cre transgene, which mediates a mosaic deletion in all mammary epithelial cell lineages, the WAP-Cre transgene was used in virgin mice to ablate TβRII expression specifically within hormone-responsive alveolar progenitors (23, 24). We have used the MMTV-PyVmT transgenic mouse line to induce mammary tumors in our mice in the context of intact or ablated TβRII expression to determine the influence of this signaling pathway on tumor progression and metastasis. The WAP-Cre transgene used in this study targeted the tumor progenitor cell population with exquisite specificity (Fig. 1*A, a–d*). At the earliest sign of hyperplasia and in the solid tumor mass, we observed a robust recombination of the Rosa26R reporter allele *in vivo*. We observed a highly significant decrease in tumor latency associated with the TβRII$^{(fl/fl);PY;WC}$ mice when compared with the TβRII$^{(fl/fl);PY}$ controls (Fig. 1*B*). TβRII$^{(fl/fl);PY;WC}$ mice also developed tumors significantly earlier than observed in the TβRII$^{(fl/fl);PY;MC}$ model (Fig. 1*B*). However, both TβRII null models had increased lung metastases at 28 days after tumor palpation when compared with the controls (Fig. 1*C*). In this study, it was necessary to sacrifice the mice at 28 days after tumor palpation as opposed to 45 days after tumor palpation in the previous study (14), due to the exceptionally large size of the conditional TβRII null tumors at this time point in the pure FVB background ($n > 12$). At this time point, the number of metastases could be quantified by counting the lesions in lung whole mounts rather than using lung weights as previously described (14). The number of metastases in the WAP-Cre and MMTV-Cre models was significantly higher than the controls. However, there was no difference in the number of metastases when comparing the TβRII$^{(fl/fl);PY;WC}$ and TβRII$^{(fl/fl);PY;MC}$ models with each other (Fig. 1*C*). Further, the total body weight, as a measure of tumor burden at the time of sacrifice, was significantly higher in TβRII$^{(fl/fl);PY;WC}$ and TβRII$^{(fl/fl);PY;MC}$ mice when compared with the TβRII$^{(fl/fl);PY}$ controls (Fig. 1*D*).

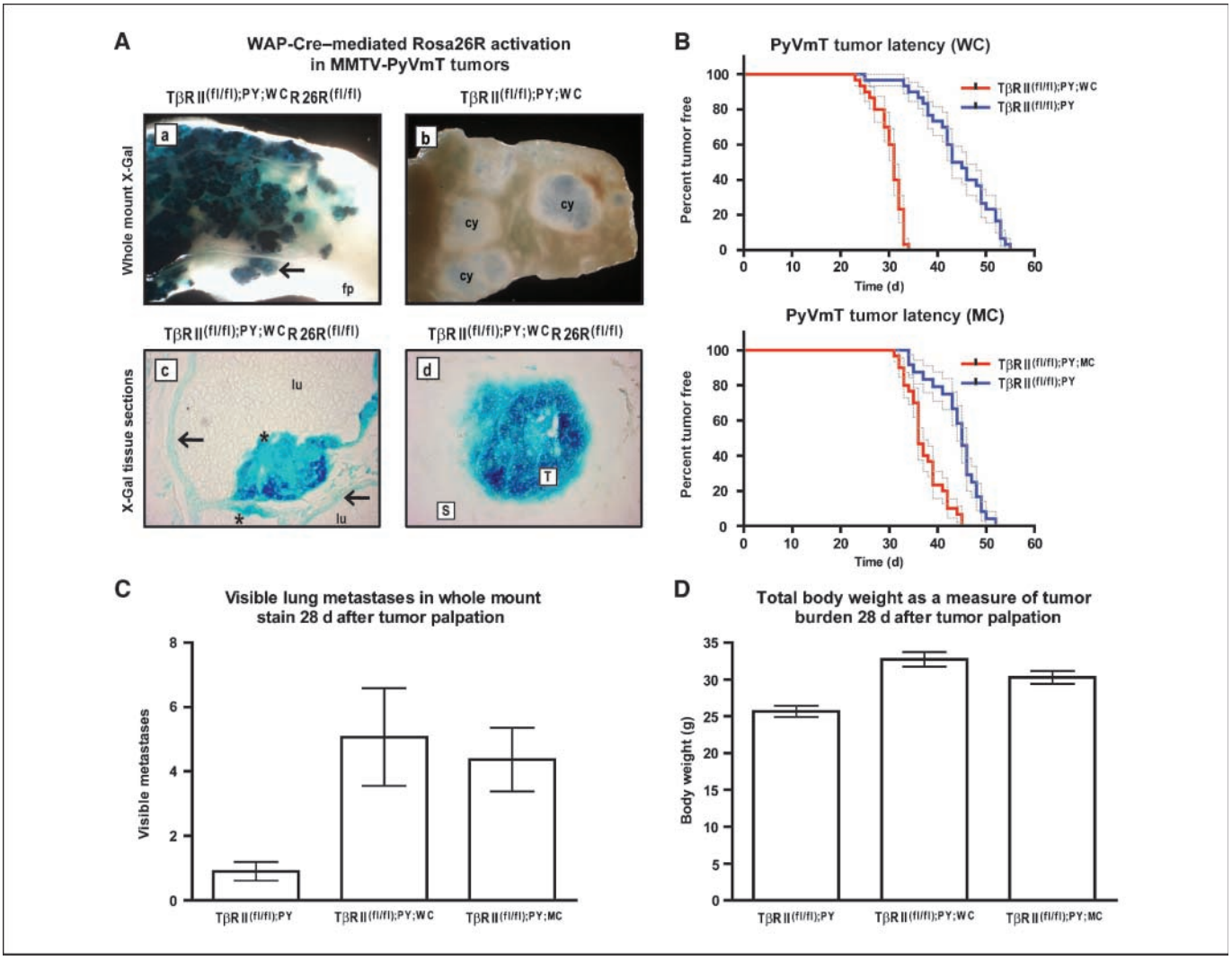

Figure 1. Loss of TGF-β signaling specifically within the mammary tumor precursor cell population significantly decreased tumor latency and promoted progression to metastasis. *A,* WAP-Cre–mediated Rosa26R activation in MMTV-PyVmT tumors. *a,* $T\beta RII^{(fl/fl);PY;WC}Rosa26R^{(fl/fl)}$ whole mount X-Gal staining of a mammary tumor 28 d after palpation. Blue staining (*arrow*) indicates recombination in lobular alveolar lesions. The mammary fat pad (*fp*) did not show evidence of recombination. *b,* $T\beta RII^{(fl/fl);PY;WC}$ whole mount X-Gal staining of a mammary tumor 28 d after palpation as a negative control. Large cysts (*cy*) were a common feature in the distal preneoplastic $T\beta RII^{(fl/fl);PY;WC}$ tumor tissue. *c* and *d,* 10-μm sections through $T\beta RII^{(fl/fl);PY;WC}Rosa26R^{(fl/fl)}$ whole mount X-Gal–stained mammary tumor tissue 28 d after palpation. *c,* in areas of hyperplasia, recombination was observed (*asterisks*; *light* and *dark blue stain*). Adjacent mammary epithelium surrounding an extended lumen (*lu*) was negative for reporter gene expression (*arrow*). *d,* solid tumor tissue (*T*) showed evidence of efficient recombination whereas adjacent stroma (*S*) was negative. *B,* Kaplan-Meier curves of the time until tumor palpation in WAP-Cre– and MMTV-Cre–mediated TβRII conditional null MMTV-PyVmT tumors. WAP-Cre–dependent loss of TβRII in MMTV-PyVmT tumors significantly decreased tumor latency. The $T\beta RII^{(fl/fl);PY;WC}$ mice developed palpable tumors with a median time of 31 d whereas the $T\beta RII^{(fl/fl);PY}$ control mice had a median time to tumor palpation of 44 d ($n = 30$ for each genotype; $P < 0.0001$). MMTV-Cre–dependent loss of TβRII in MMTV-PyVmT tumors also significantly decreased tumor latency similar to results from a previous study (14). The $T\beta RII^{(fl/fl);PY;MC}$ mice developed palpable tumors at 36 d whereas the $T\beta RII^{(fl/fl);PY}$ control mice had a median time to tumor palpation of 45 d ($n = 30$ for each genotype; $P < 0.0001$). Interestingly, when TβRII was deleted using WAP-Cre, palpable tumors were detected earlier than when using MMTV-Cre to mediate deletion ($n = 30$ for each genotype; $P < 0.0001$). The difference in littermate control groups was not significant ($n = 30$ for each group). Significance of data represented in the Kaplan-Meier curves was determined using log-rank (Mantel-Cox) and Gehan-Breslow-Wilcoxon tests for statistical significance. *C,* visible lung metastases in whole mount stains 28 d after tumor palpation. A significant increase in the number of visible metastases occurred in the $T\beta RII^{(fl/fl);PY;WC}$ and $T\beta RII^{(fl/fl);PY;MC}$ models when compared with the $T\beta RII^{(fl/fl);PY}$ controls ($n = 30$ for each genotype; $P < 0.005$ and $P < 0.0005$, respectively). The $T\beta RII^{(fl/fl);PY}$, $T\beta RII^{(fl/fl);PY;WC}$, and $T\beta RII^{(fl/fl);PY;MC}$ models had 0.9 (±0.3 SE), 5.1 (±1.5 SE), and 4.4 (±1.0 SE) metastases, respectively. There was not a significant difference when the $T\beta RII^{(fl/fl);PY;WC}$ and $T\beta RII^{(fl/fl);PY;MC}$ models were compared ($n = 30$ for each genotype). Significance for metastasis data was determined using the Wilcoxon signed rank test. *D,* total body weight at the time of sacrifice showed a significant increase in tumor burden associated with the $T\beta RII^{(fl/fl);PY;WC}$ and $T\beta RII^{(fl/fl);PY;MC}$ models when compared with $T\beta RII^{(fl/fl);PY}$ controls ($n = 20$ for each genotype; $P < 0.0001$ and $P < 0.0005$, respectively, using unpaired *t* tests). The mean body weight in the $T\beta RII^{(fl/fl);PY;WC}$ model was 32.75 g (±0.99 g) and the $T\beta RII^{(fl/fl);PY;MC}$ model had a mean body weight of 30.26 g (±0.88 g) whereas the mean body weight in the $T\beta RII^{(fl/fl);PY}$ control mice was 24.6 g (±0.6 g).

Loss of TβRII increased the abundance of cystic mammary preneoplastic hyperplasias, solid tumor tissue, pseudopapillary structures, and moderate to well-differentiated extravascular pulmonary metastases. In the absence of TβRII, we found that distal preneoplastic hyperplasias present in the MMTV-PyVmT tumors were significantly expanded (Fig. 2*A, a–c*). The hyperplastic growth predominantly involved lobular alveolar epithelium that formed well-differentiated lobular alveoli with distended lumina. The hyperplastic alveoli were often filled with a secretory product that seemed to have an abundant protein composition as indicated by eosin staining. The solid $T\beta RII^{(fl/fl);PY;WC}$ and $T\beta RII^{(fl/fl);PY;MC}$ tumor tissues showed a moderate to well-differentiated morphology

with tubular gland–like structures that were less abundant in the $T\beta RII^{(fl/fl);PY}$ controls (Fig. 2*A, d–f*). The solid $T\beta RII^{(fl/fl);PY;WC}$ and $T\beta RII^{(fl/fl);PY;MC}$ tumor tissues also showed an expansion of the stromal compartment when compared with the $T\beta RII^{(fl/fl);PY}$ controls (Fig. 2*A, d–f*). All three tumor models had an abundant pseudopapillary component; however, $T\beta RII^{(fl/fl);PY;WC}$ and $T\beta RII^{(fl/fl);PY;MC}$ pseudopapillary tissues were more cystic than in the $T\beta RII^{(fl/fl);PY}$ controls (Fig. 2*A, g–i*). The lung metastases in all three models had a moderate to well-differentiated morphology with abundant lobular alveolar structures (Fig. 2*B*, a–c).

In the absence of TβRII, mammary carcinoma cells exhibit enhanced tumor cell survival. To address the mechanisms for enhanced tumor growth and metastasis observed when TβRII was lost in carcinoma cells, we used the highly specific $T\beta RII^{(fl/fl);PY;WC}$ model in comparison with $T\beta RII^{(fl/fl);PY}$ controls. The abundant tumor volume visible by gross physical examination and histologic analyses indicated that the $T\beta RII^{(fl/fl);PY;WC}$ tumor tissues grew faster than those in the $T\beta RII^{(fl/fl);PY}$ controls. This led us to hypothesize that the carcinoma cells had a difference in the rate of proliferation or cell survival. Using phospho-histone 3 as a marker of mitosis, we were able to determine that there was not a significant difference in the rate of proliferation within individual proliferative cell clusters when TβRII was ablated in the mammary carcinoma cells (Fig. 3*A, a* and *c*). Interestingly, the proliferation in both models was predominantly localized within carcinoma cells adjacent to the fibrovascular stroma whereas no significant proliferation was observed in the stromal compartment. Conversely, we found that the $T\beta RII^{(fl/fl);PY}$ tumor tissues had an increased rate of apoptosis when compared with tissues from the $T\beta RII^{(fl/fl);PY;WC}$ model (Fig. 3*A, b* and *d*). When quantified, the relative increase in apoptosis associated with the control tumors was significant (Fig. 3*A, bottom*).

To further assess the status of total proliferation within the tumor tissue rather than within microscopic proliferative clusters, we examined the expression of TβRII, Smad3, and p-Smad3 proteins (Fig. 3*B*), in addition to several common cell cycle markers including cyclin D1, cyclin D2, cyclin D3, cyclin A, cyclin B1, cyclin-dependent kinase (Cdk)-2, and Cdk4 (Ccnd1 and Ccnd2, Fig. 3*C*). The control tissues had a significantly higher level of cyclin D1, cyclin D2, cyclin A, and cyclin B1 expression without a corresponding change in cyclin D3, Cdk2, or Cdk4 (data not shown for cyclin A, cyclin B1, cyclin D3, Cdk2, and Cdk4). This suggested

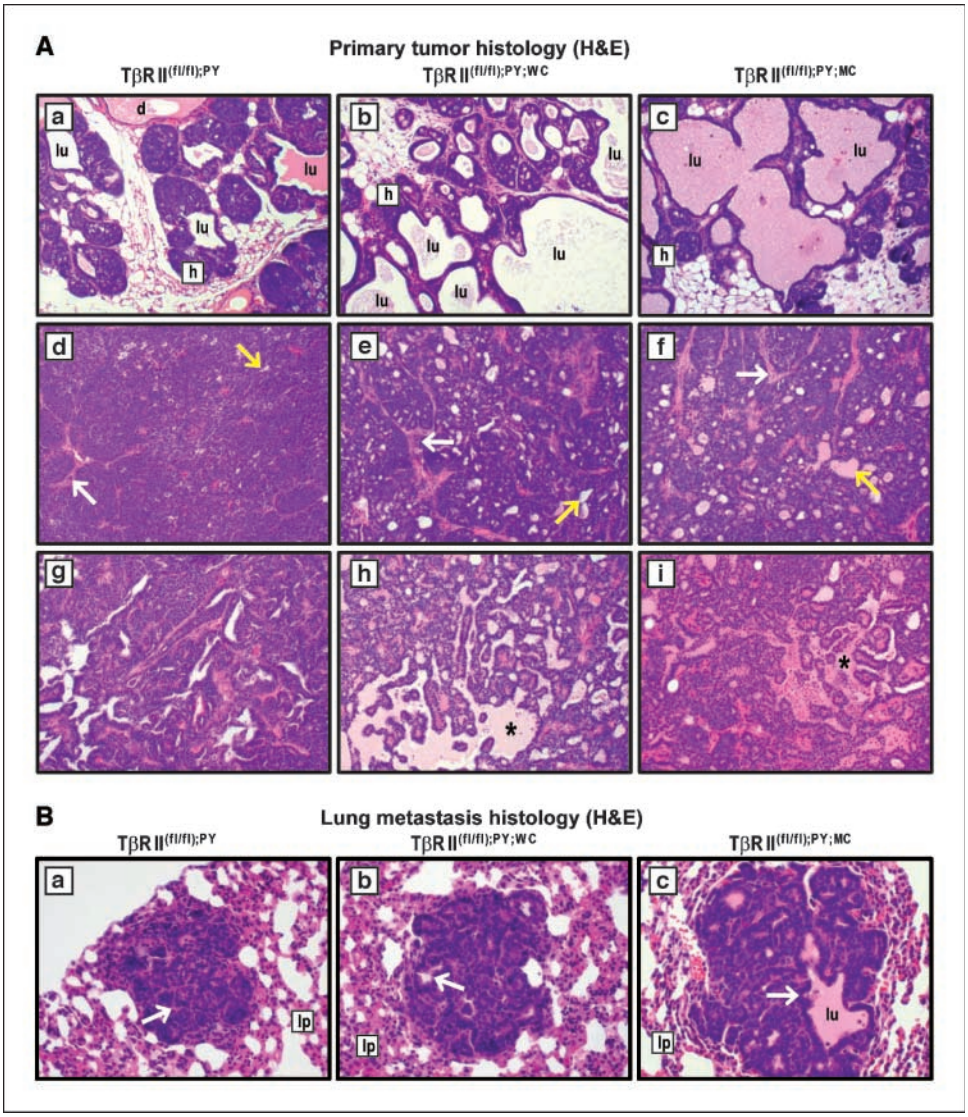

Figure 2. TGF-β regulates the expansion and differentiation of preneoplastic, solid, and pseudopapillary lesions within primary mammary tumor tissues. Histopathologic analysis of tumor tissues derived from the $T\beta RII^{(fl/fl);PY}$, $T\beta RII^{(fl/fl);PY;WC}$, and $T\beta RII^{(fl/fl);PY;MC}$ models revealed differences in three main mammary tumor compartments. *A,* the distal portion of all MMTV-PyVmT mammary tumor tissues had preneoplastic lobular-alveolar mammary hyperplasias (mammary intraepithelial neoplasia; *MIN*) with small foci of carcinoma *in situ* (*a–c*). One of the most striking histopathologic differences among the models was the presence of large cysts in hyperplastic areas associated with the $T\beta RII^{(fl/fl);PY;WC}$ and $T\beta RII^{(fl/fl);PY;MC}$ mice (*C,* cyst; *h,* hyperplasia; *lu,* lumen). The cysts often contained proteinaceous material. Adjacent and proximal to the mammary intraepithelial neoplasia region, all the tumor models had a mix of solid carcinoma *in situ* and invasive adenocarcinoma (*d–f*). Mammary tumor tissues associated with the $T\beta RII^{(fl/fl);PY;WC}$ and $T\beta RII^{(fl/fl);PY;MC}$ models were more differentiated than the $T\beta RII^{(fl/fl);PY}$ controls as determined by the increased frequency of small tubular gland–like structures throughout the solid tumor compartment (*yellow arrows*). The fibrovascular stroma was more abundant in the $T\beta RII^{(fl/fl);PY;WC}$ and $T\beta RII^{(fl/fl);PY;MC}$ models when compared with the $T\beta RII^{(fl/fl);PY}$ controls (*white arrows*). Large regions of pseudopapillary mammary hyperplasia were also observed in all three tumor models (*g–i*). The pseudopapillary regions associated with the $T\beta RII^{(fl/fl);PY;WC}$ and $T\beta RII^{(fl/fl);PY;MC}$ models were more cystic than the $T\beta RII^{(fl/fl);PY}$ controls (*asterisks*). *B,* the lung metastases in all three models had a moderate to well-differentiated morphology with abundant lobular alveolar structures (*a–c*; *arrows*). *lp,* lung parenchyma.

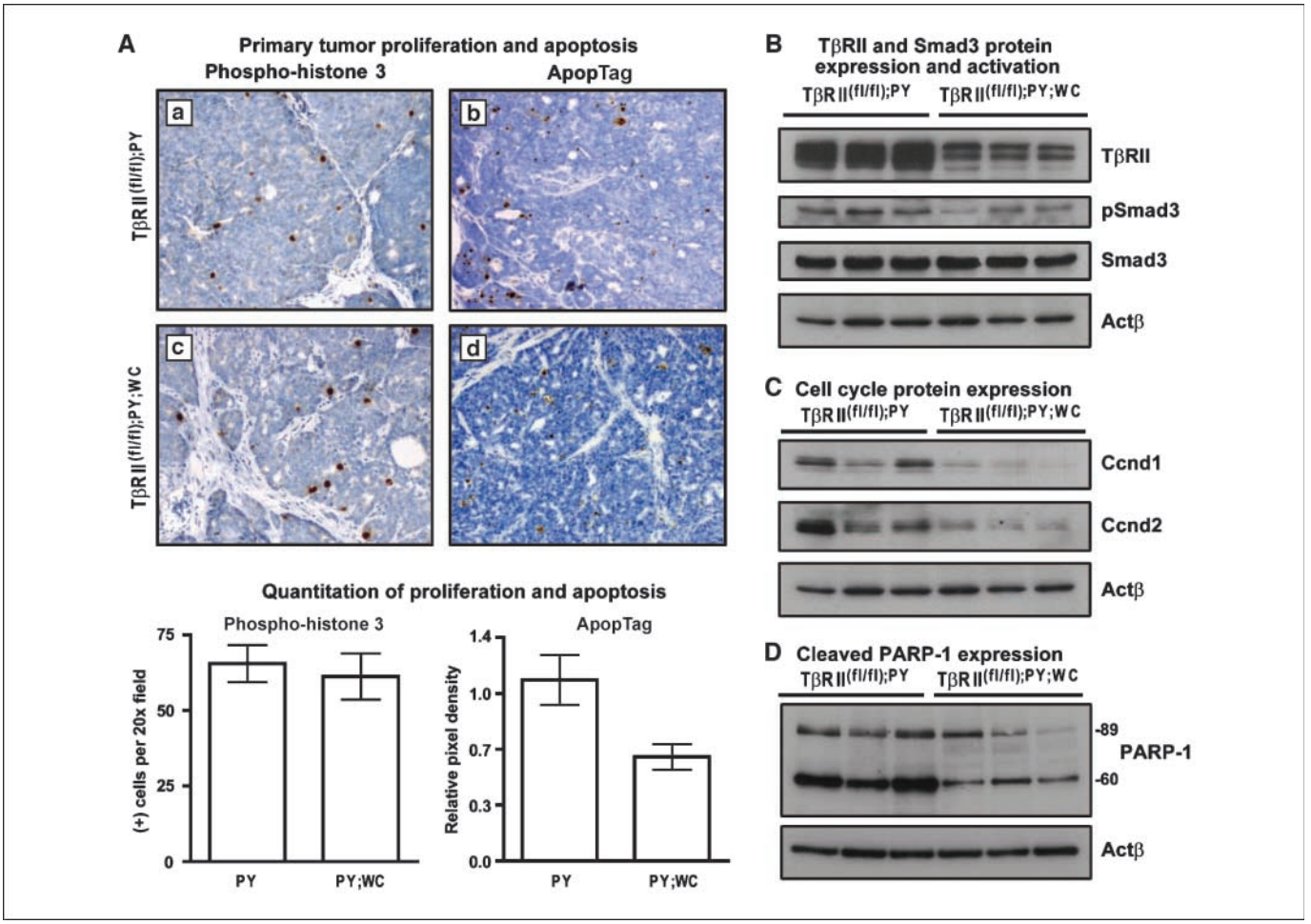

Figure 3. TGF-β signaling promotes apoptosis in primary mammary tumor tissues. *A,* primary tumor proliferation and apoptosis were analyzed using phospho-histone 3 and ApopTag immunohistochemistry, respectively. Immunohistochemistry for phospho-histone 3 revealed clusters of carcinoma cells in mitosis (*a* and *c, brown nuclei*). The $T\beta RII^{(fl/fl);PY}$ and $T\beta RII^{(fl/fl);PY;WC}$ models both showed proliferating cells in close proximity to the adjacent fibrovascular stroma. Proliferation within the stromal compartment was not observed at a significant level in either tumor model. ApopTag labeling and immunohistochemistry were done to determine the relative level of apoptotic cell death in the primary tumor tissues (*b* and *c*). *Bottom,* quantitation of proliferation and apoptosis in primary tumor tissue immunohistochemistry. No statistically significant difference was observed when the numbers of phospho-histone 3–positive cells from random proliferative clusters were quantified in the $T\beta RII^{(fl/fl);PY}$ tumor tissues and compared with those from the $T\beta RII^{(fl/fl);PY;WC}$ mice [65.4 ± 6.2 (SE) versus 61.2 ± 7.6 (SE) cells per field of view, respectively, unpaired *t* test; *n* = 6 individual tumors for each genotype and 3 random fields analyzed per tissue section]. ApopTag labeling and immunohistochemistry revealed a significant decrease in apoptosis associated with the $T\beta RII^{(fl/fl);PY;WC}$ tumor tissues when compared with the $T\beta RII^{(fl/fl);PY}$ controls [median transformed mean pixel density was 0.65 ± 0.08 (SE) versus 1.13 ± 0.16 (SE), respectively; $P < 0.01$, unpaired *t* test; *n* = 6 individual tumors for each genotype and 3 random fields analyzed per tissue section]. *B,* analysis of TβRII expression and Smad3 activation in $T\beta RII^{(fl/fl);PY}$ and $T\beta RII^{(fl/fl);PY;WC}$ mammary tumor tissues. TβRII protein was efficiently deleted in $T\beta RII^{(fl/fl);PY;WC}$ tumor tissues and this correlated with a decrease in Smad3 phosphorylation (*pSmad3*). Residual TβRII expression identified by Western blot analysis was likely due to the presence of nonepithelial cell populations within the tumor microenvironment. Total Smad3 levels were not altered in the $T\beta RII^{(fl/fl);PY;WC}$ model when compared with the $T\beta RII^{(fl/fl);PY}$ controls. *C,* cyclin D1 and cyclin D2 (annotated *Ccnd1* and *Ccnd2*) expression was significantly higher in the $T\beta RII^{(fl/fl);PY}$ control tissues. This positively correlated with cyclin A and cyclin B1 expression (data not shown). β-Actin (*Actβ*) was used as a loading control. *D,* PARP-1 cleavage was more abundant in control tissues. Typical caspase-dependent and atypical caspase-independent cleavage products were observed (bands at 89 and 60 kDa, respectively).

that a greater percentage of the cells in the $T\beta RII^{(fl/fl);PY}$ control tissue were actively proliferating (see Supplementary Fig. S1 for an illustration that relates the Western blot data to the immunohistochemistry proliferation and cell death data). We subsequently examined the expression of cleaved PARP-1 protein as an indicator of caspase activity in our tumor tissues. The control tissues had more cleaved PARP-1 expression than $T\beta RII^{(fl/fl);PY;WC}$ tissues (Fig. 3*D*). Interestingly, the presence of both typical and atypical PARP-1 cleavage products suggests that both caspase-dependent and caspase-independent pathways together contribute to the increased cell death associated with $T\beta RII^{(fl/fl);PY}$ tumor tissues *in vivo* (25).

TGF-β signaling in mammary carcinoma cells can regulate the adjacent fibrovascular stroma during tumor progression. In the tumor H&E sections, a reactive stroma was observed in the invasive tissues at 28 days after tumor palpation in the $T\beta RII^{(fl/fl);PY}$ and $T\beta RII^{(fl/fl);PY;WC}$ tumor models (Fig. 4*A, a* and *b*; higher-resolution images are available in Supplementary Fig. S2). Notably, this reactive stroma was detected in $T\beta RII^{(fl/fl);PY;WC}$ tissues as early as 9 days after tumor palpation (Fig. 4*A, c*). In addition, we observed an expansion of the stromal fibroblast cell compartment in $T\beta RII^{(fl/fl);PY;WC}$ tumors when compared with $T\beta RII^{(fl/fl);PY}$ controls (Figs. 2 *A, d–f* and 3*A, a–d*). However, it was not clear if there were phenotypic differences in the stromal fibroblasts associated with the alternate tumor models. Interestingly, most of the stroma in both models expressed vimentin (Fig. 4*B, a* and *b*); however, the stroma in $T\beta RII^{(fl/fl);PY;WC}$ tumors also had a high level of SMA expression (Fig. 4*B, c* and *d*). In the $T\beta RII^{(fl/fl);PY}$ control tumor tissues, SMA expression was predominantly localized in the stroma around

the outer margin of the tumor. In contrast, the TβRII$^{(fl/fl);PY;WC}$ model had abundant SMA expression in stromal cells adjacent to the carcinoma lobules throughout the tumor tissue.

The abundant stroma in TβRII$^{(fl/fl);PY;WC}$ tumors correlated with vascular structures in H&E sections, and we hypothesized that the abundant fibrovascular stroma may have been due to a general increase in angiogenesis. However, the endothelial cell component of the fibrovascular network did not increase in abundance when TβRII was deleted in the carcinoma epithelium. To determine the relative vascular contribution within the tumor microenvironment, we performed immunohistochemistry for vWF and CD31. vWF is often associated with macrovasculature whereas CD31 is often associated with microvascular structures, and the two markers, when analyzed together, produce distinct complementary data related to tumor vascularization. We observed no difference in vWF abundance in the areas where this protein was detected (Fig. 4*C, a* and *b*); however, we did observe a significant decrease in the amount of CD31 expression in TβRII$^{(fl/fl);PY;WC}$ tumor tissues when compared with the TβRII$^{(fl/fl);PY}$ controls (Fig. 4*C, c* and *d*). We subsequently analyzed the level of vascular endothelial growth factor-165 mRNA expression by real-time PCR and found that there was not a significant difference in the level of expression when comparing the conditional TβRII null and control tumor tissues (data not shown). These results together suggested that the stromal expansion in TβRII$^{(fl/fl);PY;WC}$ tumor tissue was not simply the result of a general increase in angiogenesis.

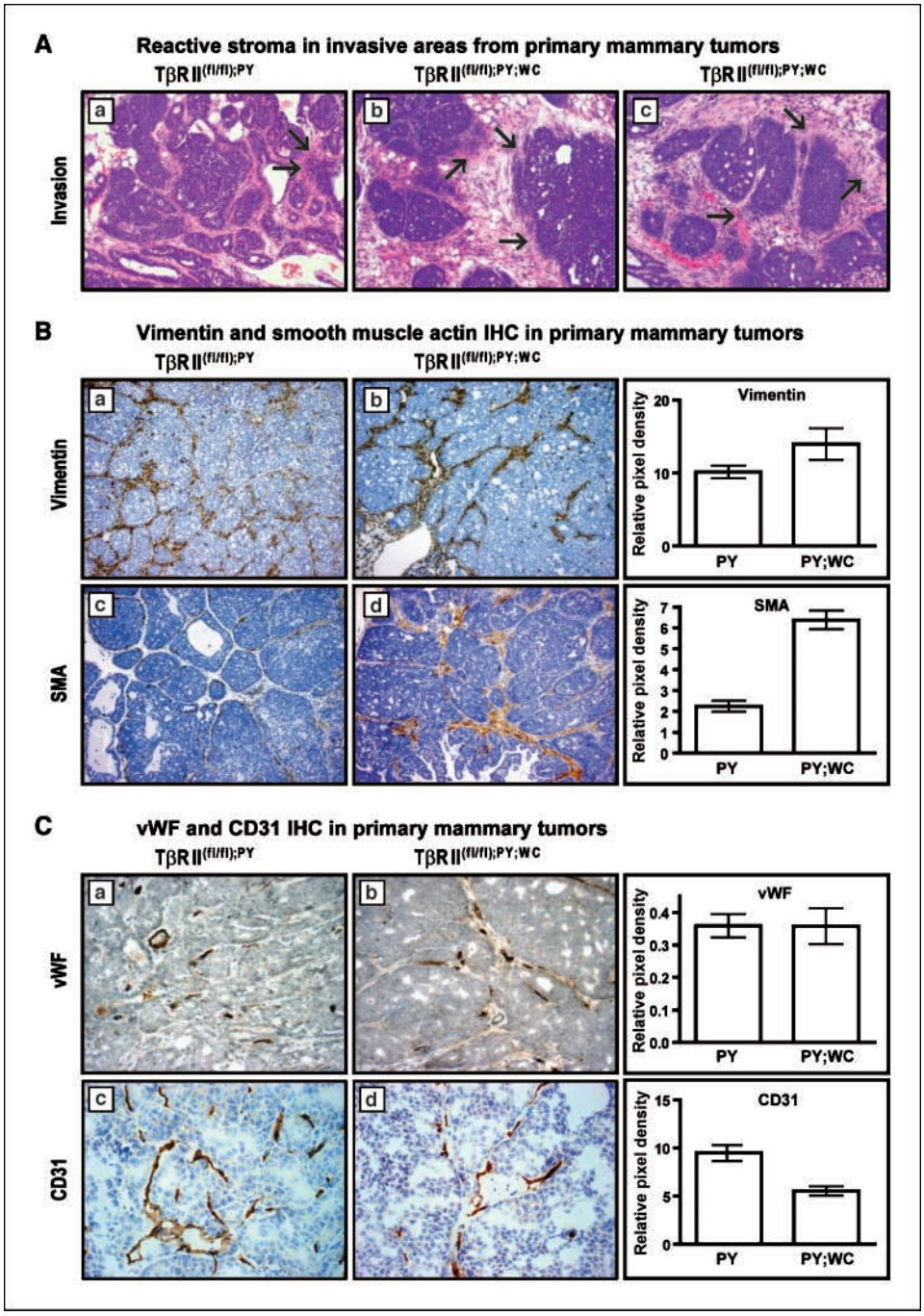

Figure 4. TGF-β signaling within mammary carcinoma cell regulates the adjacent fibrovascular stroma. *A,* invasive regions within TβRII$^{(fl/fl);PY}$ and TβRII$^{(fl/fl);PY;WC}$ tumor tissues were often associated with a reactive tumor stroma. Tumor invasion with a reactive stroma was observed in both models 28 d after palpation (*a* and *b*). However, in the TβRII$^{(fl/fl);PY;WC}$ model, invasion associated with a reactive stroma was observed as early as 9 d after tumor palpation (*c*). Vimentin expression (*B, a* and *b*), as a general marker for all fibroblast cells, was not significantly altered when comparing the TβRII$^{(fl/fl);PY}$ and TβRII$^{(fl/fl);PY;WC}$ tumor tissues [relative pixel density was 10.2 ± 0.9 (SE) versus 14.0 ± 2.1 (SE), respectively]. SMA expression (*B, c* and *d*) was significantly increased in TβRII$^{(fl/fl);PY;WC}$ tumor tissues when compared with TβRII$^{(fl/fl);PY}$ controls (relative pixel density was 6.4 ± 0.4 SE versus 2.2 ± 0.3 SE respectively; $P < 0.0001$). No significant difference was observed in vWF staining (*C, a* and *b*) when comparing the TβRII$^{(fl/fl);PY}$ and TβRII$^{(fl/fl);PY;WC}$ tumor tissues [relative pixel density was 0.35 ± 0.04 (SE) versus 0.36 ± 0.06 (SE), respectively]. CD31 staining was decreased in the TβRII$^{(fl/fl);PY;WC}$ tumor tissues (*C, c* and *d*) when compared with the TβRII$^{(fl/fl);PY}$ controls [relative pixel density was 5.5 ± 0.5 (SE) versus 9.5 ± 0.8 (SE), respectively; $P < 0.0005$]. Statistical significance for pixel density measurements was determined with unpaired *t* tests; $n = 6$ individual tumors for each genotype and 3 random fields analyzed per tissue section.

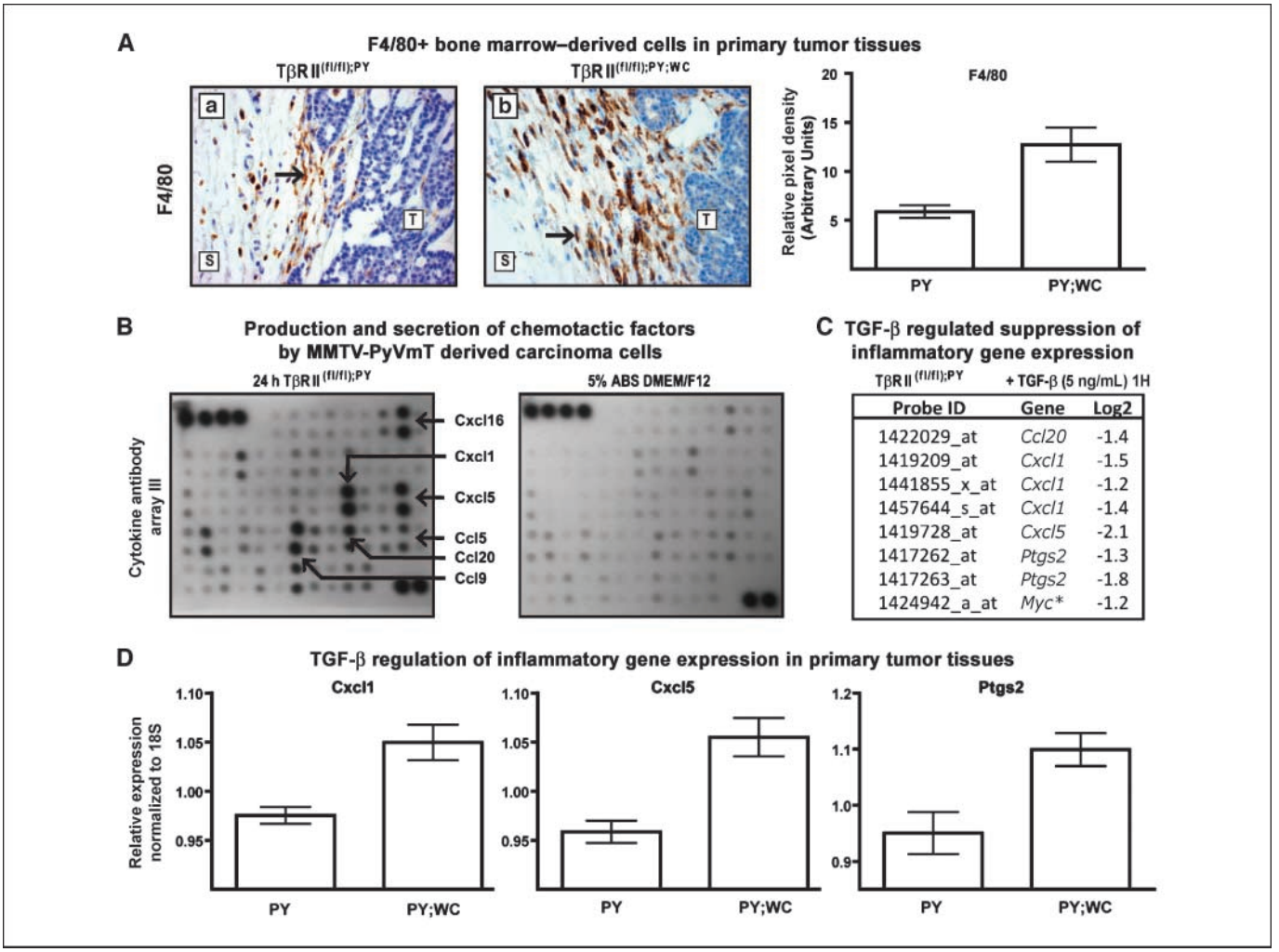

Figure 5. TGF-β signaling regulates the infiltration of F4/80$^+$ cells and correlates with the expression of genes known to promote inflammation including *Cxcl1, Cxcl5*, and *Ptgs2* (cyclooxygenase-2) in primary mammary tumor tissues. *A,* F4/80$^+$ bone marrow–derived cell infiltration into primary TβRII$^{(fl/fl);PY}$ and TβRII$^{(fl/fl);PY;WC}$ tumor tissues. F4/80 immunohistochemistry in TβRII$^{(fl/fl);PY}$ and TβRII$^{(fl/fl);PY;WC}$ tissues (*a* and *b*, respectively). The F4/80$^+$ cell population (*brown staining, arrows*) was primarily localized in the stroma (*S*) along the leading edge between the distal preneoplastic hyperplasias and adjacent solid tumor tissues (*T*). Quantitation of the F4/80$^+$ staining revealed a significant increase in F4/80$^+$ cells recruited to the TβRII$^{(fl/fl);PY;WC}$ tumor microenvironment when compared with TβRII$^{(fl/fl);PY}$ controls ($P < 0.001$). The TβRII$^{(fl/fl);PY;WC}$ tumors had a mean pixel density of 12.7 (±1.7 SE) whereas the TβRII$^{(fl/fl);PY}$ controls had a mean pixel density of 5.9 (±0.6 SE). Statistical significance was determined using an unpaired *t* test with six individual tumors for each genotype and three random fields analyzed per tissue section. *B,* identification of factors that were produced by TβRII$^{(fl/fl);PY}$ carcinoma cells using a cytokine antibody array incubated with conditioned medium that was collected after 24 h of growth. Cytokine and chemokine proteins were captured on the antibody array membrane and visualized by a secondary chemiluminescent detection. Several chemotactic factors were detected at a relatively high level in the conditioned medium from TβRII$^{(fl/fl);PY}$ carcinoma cells including Cxcl1, Cxcl5, Cxcl16, Ccl5, Ccl9, and Ccl20. Background was determined with complete growth medium alone. *C,* array data from TβRII$^{(fl/fl);PY}$ control cells versus TβRII$^{(fl/fl);PY}$ control cells + TGF-β (5 ng/mL; 1 h of stimulation) showed expression changes in genes that are known to promote inflammation. In the presence of serum, TGF-β was able to suppress the expression of *Ccl20, Cxcl1, Cxcl5*, and *Ptgs2* mRNA at a level that was similar to *c-myc*, which is a gene known to be potently repressed by TGF-β signaling. *D,* real-time PCR analysis of genes identified in *B* and *C* revealed that the loss of TGF-β signaling significantly increased the expression of *Cxcl1, Cxcl5*, and *Ptgs2* in TβRII$^{(fl/fl);PY;WC}$ primary mammary tumor tissues when compared with the TβRII$^{(fl/fl);PY}$ controls ($P < 0.0005$, $P < 0.0001$, and $P < 0.005$, respectively). No statistically significant difference was observed for *Cxcl16, Ccl5, Ccl9*, or *Ccl20* in the primary mammary tumor tissues. Eight primary mammary tumor samples for each genotype (four from the fourth inguinal gland and four from the third thoracic gland) were used to produce RNA that was used for subsequent real-time PCR experiments. Each tumor sample was tested in triplicate for each gene of interest and statistical significance was determined with unpaired *t* tests for $(1/\Delta C_t)$ values normalized to 18S and transformed to the median.

The loss of TβRII in mammary carcinoma cells can enhance recruitment of F4/80$^+$ cells to the tumor microenvironment and increase the expression of proinflammatory genes including *Cxcl1, Cxcl5* and *Ptgs2* (cyclooxygenase-2). Recent work in our laboratory has shown an abundant bone marrow–derived inflammatory cell infiltrate often associated with areas of mammary tumor invasion (26). The morphology and tissue degradation surrounding areas of inflammation suggested that a major component of this infiltrate may include F4/80$^+$ cells that have previously been implicated in the progression of human disease to malignancy (27). To analyze the abundance and localization of the F4/80$^+$ cell populations within our tumor samples, we performed immunohistochemistry (Fig. 5*A, a* and *b*). We were able to detect a significant increase in the F4/80$^+$ cell population associated with our TβRII$^{(fl/fl);PY;WC}$ tumor tissues when compared with the TβRII$^{(fl/fl);PY}$ controls.

To determine the inflammatory factors regulated by TGF-β that may influence the recruitment of the F4/80$^+$ cell population *in vivo*, it was necessary to first determine which inflammatory factors were produced by MMTV-PyVmT mammary carcinoma cells *in vitro*. We

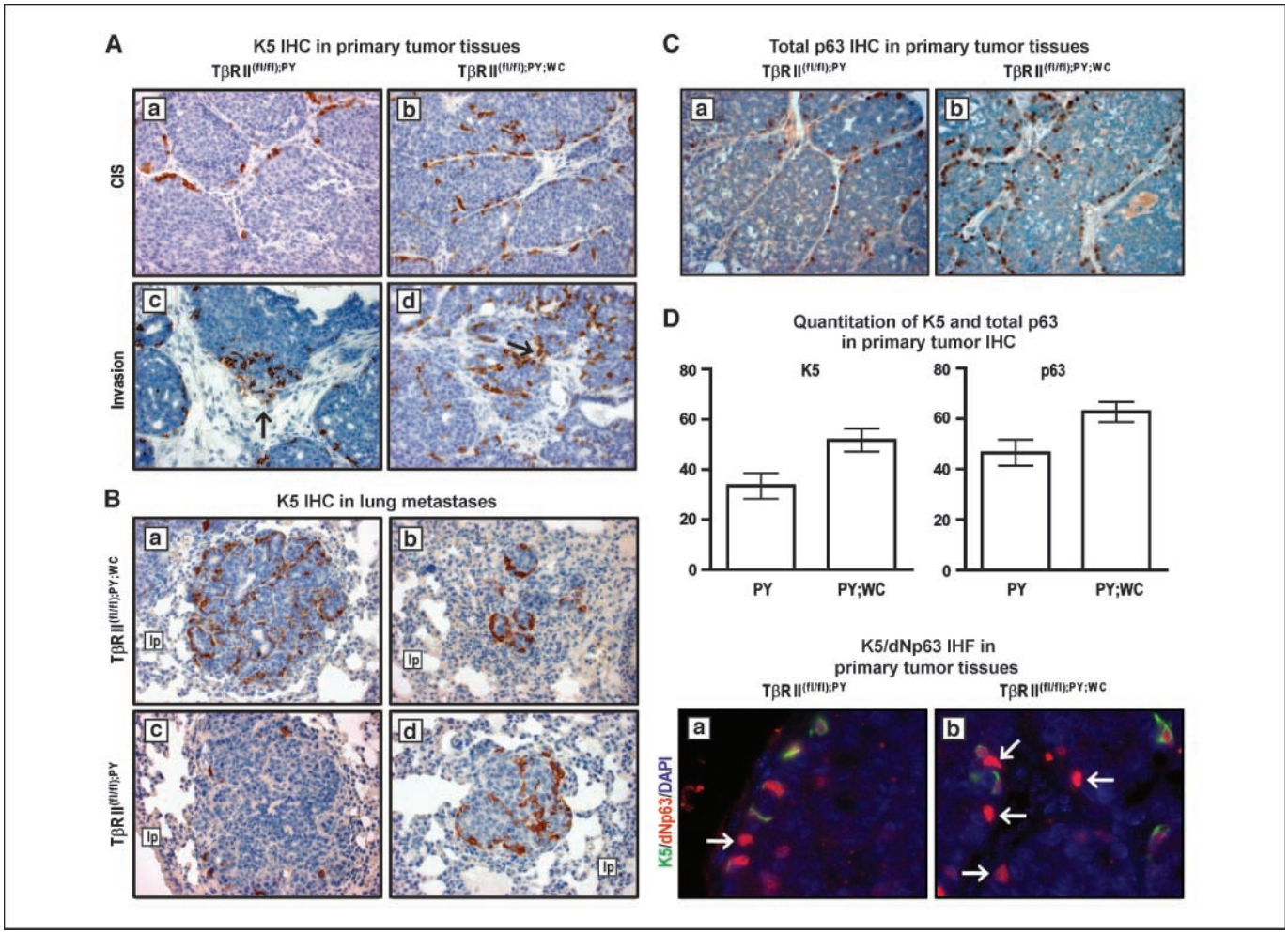

Figure 6. Loss of TGF-β signaling increased the abundance of carcinoma cell populations that express basal and myoepithelial markers in primary mammary tumors and associated lung metastases. K5-expressing carcinoma cells were enriched in $T\beta RII^{(fl/fl);PY;WC}$ tumor tissues when compared with $T\beta RII^{(fl/fl);PY}$ controls (*A* and *B*). *A,* in the primary mammary tumors [carcinoma *in situ* (*CIS*); *a* and b], K5 expression was localized in the carcinoma cell compartment adjacent to the fibrovascular stroma. K5-expressing cells constituted a minor subpopulation of invasive cells (*arrows*) present within primary mammary carcinomas (*c* and *d*). *B,* K5-expressing cells were present in lung metastases associated with the MMTV-PyVmT tumor model. Abundant K5 expression was observed in all $T\beta RII^{(fl/fl);PY;WC}$ metastases (*a* and *b*). The large (*a*) and small (*b*) metastases present in the $T\beta RII^{(fl/fl);PY;WC}$ model expressed K5 in cells that surround the lobular alveolar structures associated with the moderate and well-differentiated lung metastases. K5 expression in the $T\beta RII^{(fl/fl);PY}$ model was more variable (*c* and *d*). In the large $T\beta RII^{(fl/fl);PY}$ lung metastases, K5 expression was often sparse or not observed in stained 5-μm sections (*c*). In the small $T\beta RII^{(fl/fl);PY}$ lung metastases, K5 expression was variably expressed with some foci that had an abundant $K5^+$ cell population surrounding moderate to well-differentiated lobular alveolar structures (*d*). *C,* total p63 immunohistochemical (*IHC*) staining of primary mammary tumor tissues. The distribution of p63 in the $T\beta RII^{(fl/fl);PY}$ and $T\beta RII^{(fl/fl);PY;WC}$ tumor tissues was similar to the K5 profile. Staining was predominantly observed around the outer edge of lobules adjacent to the fibrovascular stroma. *D,* quantitation of the relative $K5^+$ and $p63^+$ cell populations within primary mammary tumor tissues. The relative pixel density for K5 was 33.4 (±5.1 SE) in the $T\beta RII^{(fl/fl);PY}$ tumor tissue versus 51.7 (±4.6 SE) in the $T\beta RII^{(fl/fl);PY;WC}$ model ($P < 0.02$). The relative pixel density for total p63 was 46.5 (±5.2 SE) in the $T\beta RII^{(fl/fl);PY}$ tumor tissue versus 62.7 (±4.0 SE) in the $T\beta RII^{(fl/fl);PY;WC}$ model ($P < 0.02$). Statistical significance for pixel density measurements was determined using unpaired *t* tests; $n = 6$ individual tumors for each genotype and 3 random fields analyzed per tissue section. *a* and *b,* K5 and δNp63 (dNp63) immunofluorescence showing that all $K5^+$ cells (*green*) were $dNp63^+$ (*red*) whereas many $dNp63^+$ cells were negative for K5 (*arrows*).

performed a cytokine and chemokine antibody array to identify factors that were produced and secreted by the carcinoma cells (Fig. 5*B*). We were able to identify Cxcl1, Cxcl5, Cxcl16, Ccl5, Ccl9, and Ccl20 as chemotactic factors that were normally produced at a significant level by MMTV-PyVmT tumor cells. To further determine which factors were highly dependent on TGF-β signaling for their regulation, we searched some of our preliminary microarray data. The microarray data set was produced to determine the changes in gene expression associated with TGF-β stimulation of control MMTV-PyVmT tumor cells for 1 hour *in vitro*. The results indicated that TGF-β decreased the expression of *Cxcl1, Cxcl5, Ccl20*, and *Ptgs2* in the MMTV-PyVmT carcinoma cells (Fig. 5*C*). The level of mRNA suppression was similar to *c-myc*, a well-known TGF-β repressed gene (28). Further, when we compared the proteins expressed by the carcinoma cells to the genes regulated by TGF-β *in vitro*, the results suggested that deleting TβRII in the carcinoma epithelium would permit an increased level of *Cxcl1, Cxcl5*, and *Ccl20* expression. We performed real-time PCR for *Cxcl1, Cxcl5, Cxcl16, Ccl5, Ccl9, Ccl20*, and *Ptgs2* using RNA from our $T\beta RII^{(fl/fl);PY}$ control and $T\beta RII^{(fl/fl);PY;WC}$ tumor tissues to determine if the results obtained *in vitro* would be relevant *in vivo*. The results indicated that *Cxcl1, Cxcl5*, and *Ptgs2* mRNA was significantly up-regulated in the $T\beta RII^{(fl/fl);PY;WC}$ tumor tissues when compared with the $T\beta RII^{(fl/fl);PY}$ controls (Fig. 5*D*). Our results suggest that in mammary carcinoma cells, when TGF-β signaling is lost, the up-regulation of proinflammatory factors can enhance the recruitment of bone marrow–derived cell populations that are known to promote tumor progression and metastasis (26, 29–31).

Basal and myoepithelial cell markers K5 and p63 are more prevalent in mammary carcinomas that lack TβRII expression *in vivo*. Currently, it is not known whether multipotent basal progenitors or lineage-committed carcinoma cells in the primary mammary tumor microenvironment give rise to distant pulmonary metastases. Our initial observations in the primary tumors and pulmonary metastases suggested that moderate to well-differentiated carcinoma cells were responsible for the distant metastases. However, we wanted to address this issue more directly using previously defined mammary cell lineage markers because it is known that the MMTV promoter/enhancer (used to drive expression of the PyVmT oncogene) can express in all mammary epithelial cell lineages including the basal cell population. As a marker for the basal and myoepithelial cell populations, we have examined K5 expression, which has previously been used to identify putative mammary progenitors, basal myoepithelium, and bona fide basaloid carcinoma cells *in situ* (32–34). K5 expression was more abundant in the epithelial cell compartment of $T\beta RII^{(fl/fl);PY;WC}$ tumor tissues when compared with $T\beta RII^{(fl/fl);PY}$ controls (Fig. 6*A, a* and *b*). In the $T\beta RII^{(fl/fl);PY}$ control tissues, K5 expression was predominantly limited to small lobules (Supplementary Fig. S3, *a*). However, the $T\beta RII^{(fl/fl);PY;WC}$ tumors had a relatively high number of $K5^+$ cells throughout the tissue regardless of individual lobule size (Supplementary Fig. S3, *b*). The K5 staining, when present, in both tumor models predominantly localized at the outer edge of each lobule directly adjacent to the stroma (Fig. 6*A, a* and *b*; Supplementary Fig. S3, *a* and *b*).

We observed invasive areas in both tumor models that contained $K5^+$ cells (Fig. 6*A, c* and *d*). Due to the moderate and well-differentiated lobular alveolar morphology of the lung metastases in both tumor models, we did not expect that $K5^+$ cells would be present in the metastatic tumor tissues. However, we did entertain the possibility. To address this issue, we performed immunohistochemistry and immunofluorescence for K5 on the $T\beta RII^{(fl/fl);PY}$ and $T\beta RII^{(fl/fl);PY;WC}$ lung metastases (Fig. 6*B, a–d*). Interestingly, in the $T\beta RII^{(fl/fl);PY;WC}$ tumor model, K5 expression was abundant in the lung metastases and localized in the same pattern observed in the primary lesions (Fig. 6*B, a* and *b*). Every metastatic nodule identified in the $T\beta RII^{(fl/fl);PY;WC}$ model was associated with a prevalent $K5^+$ cell population. In contrast, the $T\beta RII^{(fl/fl);PY}$ controls had fewer $K5^+$ cells in the metastatic foci when present (Fig. 6*B, c* and *d*), and in many cases the $K5^+$ cells were absent.

To determine if the $K5^+$ population could be further stratified using additional basal and myoepithelial cell lineage markers, we performed immunofluorescence colocalization with SMA and p63. Some of the $K5^+$ cells were SMA^+; however, many of the $K5^+$ cells were SMA^- (Supplementary Fig. S4*A, a–d*). The SMA^+ cells likely represented differentiated myoepithelial cells whereas the SMA^- population did not express this differentiation marker. *p63* gene expression, like *K5*, has been associated with basal and myoepithelial cell populations (35, 36). We therefore performed immunohistochemistry for total p63 to determine if it was enriched to a similar extent as K5 (Fig. 6*C, a* and *b*). The p63 stain had a similar spatial distribution as K5; however, quantitation of the staining suggested that there were more $p63^+$ cells than $K5^+$ cells (Fig. 6*D, graphs*). Due to the putative difference in K5 and total p63 abundance, we performed immunofluorescence to colocalize the two proteins in our tumor tissues. It is known that there are at least six alternate p63 isoforms, and we therefore limited our colocalization analyses to the δNp63 (dNp63) isoforms that have previously been associated with the early stages of progenitor cell differentiation (Fig. 6*D, a* and *b*; refs. 36–38). Every $K5^+$ cell was also $dNp63^+$. However, we also observed $dNp63^+$ $K5^-$ cells in all primary and metastatic tumor tissues analyzed. These results suggested that the neoplastic $K5^+$ $dNp63^+$ cells represented a distinct MMTV-PyVmT carcinoma cell subpopulation. Next, we verified that the $K5^+$ cells did not express markers indicative of genuine luminal cells. We performed immunofluorescence colocalization of K5 and K8, a known marker for the luminal cell lineage found within ducts and alveoli (Supplementary Fig. S4*B, a–d*; ref. 34). The $K5^+$ cell population was absolutely distinct from the $K8^+$ cell population, indicating that the K5 staining represented a subset of carcinoma cells rather than a trait acquired by partially differentiated carcinoma cells of ductal or lobular alveolar origin.

Discussion

TGF-β mediated regulation of apoptosis. TGF-β in normal epithelium is known to induce arrest of the cell cycle in G_1, and during early tumor progression it has been suggested that this cytostatic regulation is a major contribution to carcinoma cell–autonomous TGF-β–mediated tumor suppression (7). However, our data now suggest that the apoptotic response to TGF-β signaling also plays a significant role in early mammary tumor suppression. The decrease in both typical and atypical PARP-1 cleavage products associated with the $T\beta RII^{(fl/fl);PY;WC}$ tumor tissue suggests that both the extrinsic and intrinsic caspase-dependent and caspase-independent cell death pathways are impaired in the absence of TGF-β signaling (25). The inhibition of apoptosis is an important consideration with regard to clinical treatment of cancer involving radiation or chemotherapy (39, 40). Radiation or conventional chemotherapies are often used to eliminate cancer cells that have been left behind during surgery, those that remain in circulation at the time of surgical resection, or those that have already metastasized. Our current data suggest that radiation and chemotherapies designed to induce carcinoma cell death may be less effective in eliminating the cells that have diminished TGF-β signaling during tumor progression. We are currently testing this hypothesis *in vitro* and *in vivo*.

Carcinoma-associated fibroblast cell populations can significantly regulate tumor progression. It is now well known that carcinoma-associated fibroblasts can contribute to tumor progression (41–43). However, it is not known specifically which endogenous fibroblast subpopulations are involved in the regulation of adjacent carcinoma progression. Previously, it has been shown that individual fibroblast populations can be differentially classified based on their unique molecular signatures (44). The unique signatures obtained by mRNA expression profiling suggested that, much like epithelial or myeloid cells, there may be distinct fibroblast subpopulations present within each tissue type. Further, a recent study that used the vimentin, type I collagen, FSP (S100A4), α-SMA, platelet-derived growth factor receptor β, and NG2 markers to examine fibroblast heterogeneity within mammary and pancreatic carcinomas indicated that several distinct fibroblast subpopulations could be identified and quantified within the tumor microenvironment (45). Together, these results provide evidence for a fibroblast contribution to tumor initiation and progression while suggesting that individual subpopulations of fibroblasts may play similar or alternate roles that together contribute to the regulation of tumor progression.

In our system, the difference in total stromal abundance, SMA expression, and macrovascular/microvascular phenotype suggests that TGF-β signaling within the carcinoma cell significantly regulates the composition of adjacent fibrovascular stroma in the

mammary tumor microenvironment. Currently, we do not know what factors the SMA^+ fibroblast-like cells are producing or how these unknown factors affect tumor progression. It is known, however, that myofibroblasts are often associated with the leading edge of invasive tumors, and it has been suggested that they promote tumor progression (6). In our study, we observed SMA^+ staining in the stroma associated with most of the invasive areas (data not shown), and this further suggests that a SMA^+ tumor reactive stroma may be involved in early invasion thereby promoting progression to metastasis.

Tumor-associated macrophages significantly contribute to tumor progression and metastasis. Tumor-associated macrophages (TAM) are known to significantly regulate normal mammary development and tumor progression (29–31). The F4/80 antigens have been widely used for the identification of macrophage lineage cell populations *in vivo* (30). Clinically, identification of TAM cell populations in invasive breast carcinoma tissue has been correlated with a poor prognosis that includes reduced relapse-free and overall survival (27). Monocytes can be recruited to the tumor microenvironment where they undergo limited macrophage differentiation and significantly contribute to tumor progression. It has been suggested that TAMs contribute to at least six central processes involved in tumor progression including tumor cell invasion, inflammation, matrix remodeling, intravasation, seeding at distant sites, and promotion of angiogenesis (31). Interestingly, it has been shown that carcinoma cells and TAMs have the ability to migrate together in response to the reciprocal expression of colony-stimulating factor-1 and epidermal growth factor, respectively (46). Functionally, based on the literature, it is clear that TAMs promote tumor progression and metastasis; therefore, it is important to determine the factors produced by tumor cells that regulate the recruitment of TAMs to the tumor microenvironment. In addition to previously described TAMs, recent work in our laboratory has now shown that TGF-β signaling in carcinoma cells can significantly regulate chemokine-dependent recruitment of additional bone marrow–derived myeloid cell lineages that contribute to tumor progression and metastasis (26).

Chemokines are a group of proteins that potently promote tumor inflammation by recruiting host cells to the organ where they are expressed. The data generated in this study suggest that, *in vivo*, carcinoma cell–specific loss of TGF-β signaling increases *Cxcl1, Cxcl5*, and *Ptgs2* (cyclooxygenase-2) gene expression that correlates with increased infiltration of $F4/80^+$ bone marrow–derived cells to the tumor microenvironment. Further, we have shown that the TGF-β–dependent chemokine expression observed in the tumor microenvironment likely involves direct tumor cell–autonomous regulation of gene expression by TGF-β, through experiments showing suppression of *Cxcl1, Cxcl5*, and *Ptgs2* when carcinoma cells were treated with TGF-β1 *in vitro*.

K5 expression is correlated with a poor clinical prognosis in human breast cancer. In the normal mammary gland, a common progenitor cell can differentiate to produce lubolar alveolar and ductal epithelium in addition to basal myoepithelium (47). Each of these cell types expresses a different subset of proteins that are often used to identify its lineage (34, 35, 48). The basal and myoepithelial cell populations in mammary tissue are known to express K5. Importantly, *K5* gene expression significantly correlates with a basal cell subtype classification that is known to have a poor prognosis in human breast cancer (49, 50). In a study composed of 611 human breast cancer samples, K5/K6 protein expression in node-negative breast tumor tissue was a prognostic factor for poor clinical outcome, independent of primary tumor size or grade (33). In a similar study composed of 1,944 human breast cancer samples, K5/K6 protein expression was correlated with poor prognosis in addition to loss of ER expression and early age of tumor onset (32).

The tumors produced in our mouse models were predominantly adenocarcinoma; however, the data indicate that the loss of TGF-β signaling in mammary tumor precursors can enrich for a $K5^+$ cell population. The presence of $K5^+$ cells did not classify the total tumor tissue as a basaloid subtype; however, it did indicate that there was an increased number of carcinoma cells with basaloid characteristics in tissues lacking TβRII expression. Many of the $K5^+$ cells in our tumor tissues were negative for SMA, suggesting that they were less differentiated than the cells expressing SMA. In addition, all of the $K5^+$ cells were $dNp63^+$ and negative for the luminal epithelial cell marker K8. Together the SMA, K8, and dNp63 colocalization data suggest that the $K5^+$ carcinoma cell population includes a poorly differentiated subpopulation of cells that may contribute to tumor progression and metastasis in the absence of TβRII signaling *in vivo*. Further, our analyses revealed that the $K5^+$ $p63^+$ cell population was enriched within the corresponding pulmonary metastases. It is our current hypothesis that some of the $K5^+$ cells are carcinoma progenitors that can metastasize and then divide asymmetrically, resulting in progenitor expansion and amplification of differentiated progeny. In subsequent experiments, it would be informative to determine if the $K5^+$ cells express additional markers such as CD44 or CD24 that will permit sorting to test if they can function as self-renewing carcinoma progenitors.

Our current results indicate that when TGF-β signaling is lost in the mammary tumor microenvironment, several factors should be considered including the effect on carcinoma cell apoptosis, regulation of adjacent stromal fibrovascular cell populations, carcinoma cell lineage selection, regulation of inflammatory gene expression, and infiltration of tumor promoting bone marrow–derived cell populations to the tumor microenvironment. It is likely that, together, these factors significantly contribute to the TGF-β–mediated regulation of early tumor progression and metastasis.

Acknowledgments

Received 9/21/2007; revised 12/3/2007; accepted 12/19/2007.

Grant support: NIH grants CA085492-06, CA102162, and CA126505 and the T.J. Martell Foundation.

The costs of publication of this article were defrayed in part by the payment of page charges. This article must therefore be hereby marked *advertisement* in accordance with 18 U.S.C. Section 1734 solely to indicate this fact.

We would like thank Dr. Jeffrey Rosen, Dr. Gertraud Robinson, and all the members of the Moses laboratory for critical reading and essential discussions related to the data presented in this article.

References

1. Akhurst RJ, Derynck R. TGF-β signaling in cancer—a double-edged sword. Trends Cell Biol 2001;11:S44–51.
2. Derynck R, Akhurst RJ, Balmain A. TGF-β signaling in tumor suppression and cancer progression. Nat Genet 2001;29:117–29.
3. Derynck R, Zhang YE. Smad-dependent and Smad-independent pathways in TGF-β family signalling. Nature 2003;425:577–84.
4. Bierie B, Moses HL. Tumour microenvironment. TGFβ: the molecular Jekyll and Hyde of cancer. Nat Rev Cancer 2006;6:506–20.
5. Levy L, Hill CS. Alterations in components of the TGF-β superfamily signaling pathways in

human cancer. Cytokine Growth Factor Rev 2006;17:41–58.
6. Bierie B, Moses HL. TGF-β and cancer. Cytokine Growth Factor Rev 2006;17:29–40.
7. Siegel PM, Massague J. Cytostatic and apoptotic actions of TGF-β in homeostasis and cancer. Nat Rev Cancer 2003;3:807–21.
8. Gorska AE, Jensen RA, Shyr Y, Aakre ME, Bhowmick NA, Moses HL. Transgenic mice expressing a dominant-negative mutant type II transforming growth factor-β receptor exhibit impaired mammary development and enhanced mammary tumor formation. Am J Pathol 2003;163:1539–49.
9. Lenferink AE, Magoon J, Pepin MC, Guimond A, O'Connor-McCourt MD. Expression of TGF-β type II receptor antisense RNA impairs TGF-β signaling *in vitro* and promotes mammary gland differentiation *in vivo*. Int J Cancer 2003;107:919–28.
10. Siegel PM, Shu W, Cardiff RD, Muller WJ, Massague J. Transforming growth factor β signaling impairs Neu-induced mammary tumorigenesis while promoting pulmonary metastasis. Proc Natl Acad Sci U S A 2003;100:8430–5.
11. Muraoka-Cook RS, Shin I, Yi JY, et al. Activated type I TGFβ receptor kinase enhances the survival of mammary epithelial cells and accelerates tumor progression. Oncogene 2006;25:3408–23.
12. Oft M, Heider KH, Beug H. TGFβ signaling is necessary for carcinoma cell invasiveness and metastasis. Curr Biol 1998;8:1243–52.
13. Oft M, Peli J, Rudaz C, Schwarz H, Beug H, Reichmann E. TGF-β1 and Ha-Ras collaborate in modulating the phenotypic plasticity and invasiveness of epithelial tumor cells. Genes Dev 1996;10:2462–77.
14. Forrester E, Chytil A, Bierie B, et al. Effect of conditional knockout of the type II TGF-β receptor gene in mammary epithelia on mammary gland development and polyomavirus middle T antigen induced tumor formation and metastasis. Cancer Res 2005;65:2296–302.
15. Guy CT, Cardiff RD, Muller WJ. Induction of mammary tumors by expression of polyomavirus middle T oncogene: a transgenic mouse model for metastatic disease. Mol Cell Biol 1992;12:954–61.
16. Andrechek ER, Hardy WR, Siegel PM, Rudnicki MA, Cardiff RD, Muller WJ. Amplification of the neu/erbB-2 oncogene in a mouse model of mammary tumorigenesis. Proc Natl Acad Sci U S A 2000;97:3444–9.
17. Wagner KU, Wall RJ, St-Onge L, et al. Cre-mediated gene deletion in the mammary gland. Nucleic Acids Res 1997;25:4323–30.
18. Chytil A, Magnuson MA, Wright CV, Moses HL. Conditional inactivation of the TGF-β type II receptor using Cre:Lox. Genesis 2002;32:73–5.
19. Soriano P. Generalized lacZ expression with the ROSA26 Cre reporter strain. Nat Genet 1999;21:70–1.
20. Ruddy MJ, Shen F, Smith JB, Sharma A, Gaffen SL. Interleukin-17 regulates expression of the CXC chemokine LIX/CXCL5 in osteoblasts: implications for inflammation and neutrophil recruitment. J Leukoc Biol 2004;76:135–44.
21. Lean JM, Murphy C, Fuller K, Chambers TJ. CCL9/MIP-1γ and its receptor CCR1 are the major chemokine ligand/receptor species expressed by osteoclasts. J Cell Biochem 2002;87:386–93.
22. Brown SL, Riehl TE, Walker MR, et al. Myd88-dependent positioning of Ptgs2-expressing stromal cells maintains colonic epithelial proliferation during injury. J Clin Invest 2007;117:258–69.
23. Ahmed F, Wyckoff J, Lin EY, et al. GFP expression in the mammary gland for imaging of mammary tumor cells in transgenic mice. Cancer Res 2002;62:7166–9.
24. Henry MD, Triplett AA, Oh KB, Smith GH, Wagner KU. Parity-induced mammary epithelial cells facilitate tumorigenesis in MMTV-neu transgenic mice. Oncogene 2004;23:6980–5.
25. Bey EA, Bentle MS, Reinicke KE, et al. An NQO1- and PARP-1-mediated cell death pathway induced in non-small-cell lung cancer cells by β-lapachone. Proc Natl Acad Sci U S A 2007;104:11832–7.
26. Yang L, Huang J, Ren X, et al. Abrogation of TGFb signaling in mammary carcinomas recruits Gr-1+CD11b+ myeloid cells that promote metastasis. Cancer Cell 2008;13:23–35.
27. Leek RD, Lewis CE, Whitehouse R, Greenall M, Clarke J, Harris AL. Association of macrophage infiltration with angiogenesis and prognosis in invasive breast carcinoma. Cancer Res 1996;56:4625–9.
28. Pietenpol JA, Holt JT, Stein RW, Moses HL. Transforming growth factor β1 suppression of c-myc gene transcription: role in inhibition of keratinocyte proliferation. Proc Natl Acad Sci U S A 1990;87:3758–62.
29. Coussens LM, Werb Z. Inflammation and cancer. Nature 2002;420:860–7.
30. Lewis CE, Pollard JW. Distinct role of macrophages in different tumor microenvironments. Cancer Res 2006;66:605–12.
31. Condeelis J, Pollard JW. Macrophages: obligate partners for tumor cell migration, invasion, and metastasis. Cell 2006;124:263–6.
32. Abd El-Rehim DM, Pinder SE, Paish CE, et al. Expression of luminal and basal cytokeratins in human breast carcinoma. J Pathol 2004;203:661–71.
33. van de Rijn M, Perou CM, Tibshirani R, et al. Expression of cytokeratins 17 and 5 identifies a group of breast carcinomas with poor clinical outcome. Am J Pathol 2002;161:1991–6.
34. Mikaelian I, Hovick M, Silva KA, et al. Expression of terminal differentiation proteins defines stages of mouse mammary gland development. Vet Pathol 2006;43:36–49.
35. Buono KD, Robinson GW, Martin C, et al. The canonical Notch/RBP-J signaling pathway controls the balance of cell lineages in mammary epithelium during pregnancy. Dev Biol 2006;293:565–80.
36. Barbareschi M, Pecciarini L, Cangi MG, et al. p63, a p53 homologue, is a selective nuclear marker of myoepithelial cells of the human breast. Am J Surg Pathol 2001;25:1054–60.
37. Candi E, Dinsdale D, Rufini A, et al. TAp63 and ΔNp63 in cancer and epidermal development. Cell Cycle 2007;6:274–85.
38. Senoo M, Pinto F, Crum CP, McKeon F. p63 Is essential for the proliferative potential of stem cells in stratified epithelia. Cell 2007;129:523–36.
39. Pommier Y, Sordet O, Antony S, Hayward RL, Kohn KW. Apoptosis defects and chemotherapy resistance: molecular interaction maps and networks. Oncogene 2004;23:2934–49.
40. Fulda S, Debatin KM. Extrinsic versus intrinsic apoptosis pathways in anticancer chemotherapy. Oncogene 2006;25:4798–811.
41. Barcellos-Hoff MH, Ravani SA. Irradiated mammary gland stroma promotes the expression of tumorigenic potential by unirradiated epithelial cells. Cancer Res 2000;60:1254–60.
42. Hayward SW, Wang Y, Cao M, et al. Malignant transformation in a nontumorigenic human prostatic epithelial cell line. Cancer Res 2001;61:8135–42.
43. Sakakura T, Sakagami Y, Nishizuka Y. Accelerated mammary cancer development by fetal salivary mesenchyma isografted to adult mouse mammary epithelium. J Natl Cancer Inst 1981;66:953–9.
44. Chang HY, Chi JT, Dudoit S, et al. Diversity, topographic differentiation, and positional memory in human fibroblasts. Proc Natl Acad Sci U S A 2002;99:12877–82.
45. Sugimoto H, Mundel TM, Kieran MW, Kalluri R. Identification of fibroblast heterogeneity in the tumor microenvironment. Cancer Biol Ther 2006;5:1640–6.
46. Wang W, Goswami S, Sahai E, Wyckoff JB, Segall JE, Condeelis JS. Tumor cells caught in the act of invading: their strategy for enhanced cell motility. Trends Cell Biol 2005;15:138–45.
47. Hennighausen L, Robinson GW. Information networks in the mammary gland. Nat Rev Mol Cell Biol 2005;6:715–25.
48. Shillingford JM, Miyoshi K, Robinson GW, et al. Proteotyping of mammary tissue from transgenic and gene knockout mice with immunohistochemical markers: a tool to define developmental lesions. J Histochem Cytochem 2003;51:555–65.
49. Sorlie T, Tibshirani R, Parker J, et al. Repeated observation of breast tumor subtypes in independent gene expression data sets. Proc Natl Acad Sci U S A 2003;100:8418–23.
50. Perou CM, Sorlie T, Eisen MB, et al. Molecular portraits of human breast tumours. Nature 2000;406:747–52.